Preliminary research on safety of induced seismicity at carbon sequestration sites

* Chi-Jen Chen [1,2]
[1] Graduate Institute of Applied Geology, National Central University, Taoyuan, Taiwan
[2]National Atomic Research Institute (stevenkane@nari.org.tw)

ABSTRACT

Geological carbon sequestration is a critical step towards achieving Taiwan's net-zero emissions by 2050. The issues of induced seismicity and the reactivation of fractures as potential leakage paths due to the injection of supercritical CO2 into geological formations must be thoroughly investigated to gain public acceptance for carbon sequestration sites. This study uses the Changhua Coastal Park pilot site to establish two geological models and develop corresponding numerical simulation techniques. It examines whether CO2 injection impacts the stability of adjacent blind fault. The numerical simulations, conducted with three-dimensional distinct element method software, calculate the influence range of pressure increments and compare the differences between the two geological models. Two-phase flow is implemented in fully coupled numerical simulations based on the Buckley–Leverett equation.

Keywords: geological carbon sequestration, pressure buildup, earthquake, hydromechanical coupling, 3DEC

1. Introduction

Achieving net-zero emissions by 2050 has become a national commitment for Taiwan, in alignment with global climate strategies. Geological carbon sequestration (GCS) is recognized as a key negative-emission technology to meet this target (IEA, 2017). However, the potential for induced seismicity, triggered by the injection of supercritical CO_2 into subsurface formations, remains a significant challenge for public acceptance and regulatory approval (Mortezaei and Vahedifard, 2015).

In the risk and environmental impact assessment of carbon storage, faults and fractures are among the critical pathways for potential CO_2 leakage. Carbon dioxide may migrate upward along previously unidentified faults, breaching the caprock seal, or it may leak through pre-existing sealing faults whose permeability increases due to pressure buildup. Such leakage can pose risks to drinking water resources and subsurface ecosystems (IPCC, 2005). In addition, carbon storage operations may induce seismic events, with the maximum estimated magnitude reaching up to 5.7 (Verdon, J.P., 2014). Therefore, both the potential public impact of induced seismicity and its effects on the long-term integrity of the caprock have become key topics in recent research.

Taiwan is located along the seismically active Pacific Ring of Fire. Several NE-SW trending normal faults are distributed across the Taiwan Strait. The distribution of active faults is primarily located between the Western Foothills and the coastal plains of western Taiwan. The development of carbon storage sites in Taiwan will inevitably require a rigorous assessment of the influence of faults and seismic hazards.

Geomechanical processes are among the key technical issues in geological carbon storage. As shown in Fig. 1, abandoned wells or small-scale subsurface faults may exist near storage sites. The injected CO_2 plume can alter the pore pressure within the formation (either the reservoir or caprock), potentially leading to deformation of adjacent strata, microseismicity, or reactivation of pre-existing faults.

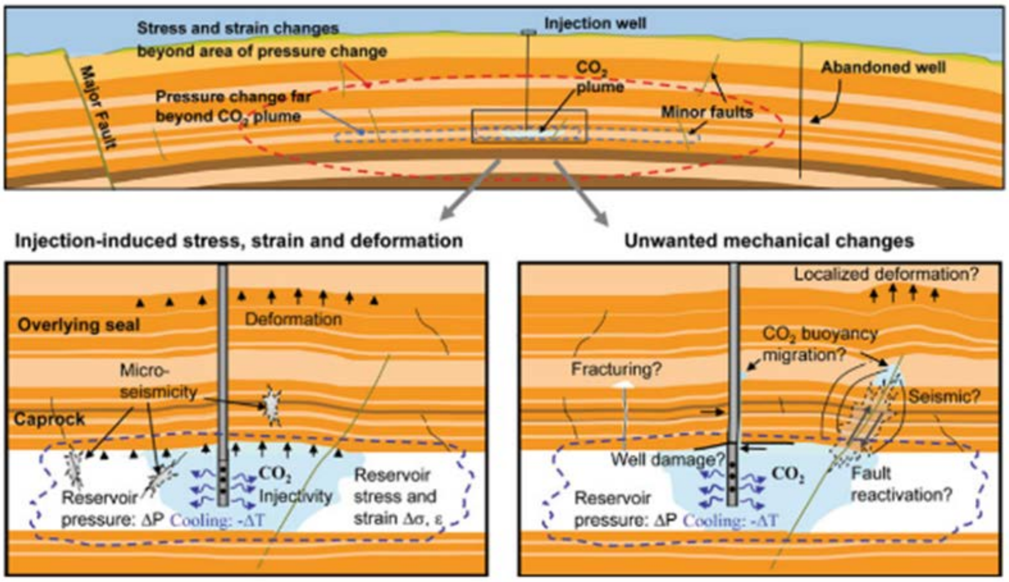

Fig. 1. The key technical issues of geomechanical processes in geological carbon storage (Rutqvist, 2012).

Mortezaei and Vahedifard (2015) employed COMSOL Multiphysics to perform a two-dimensional thermo-hydro-mechanical (THM) coupled simulation of CO_2 storage. Their study assessed stress changes and deformation within the reservoir, caprock, and fault zones. The model incorporated a fault with dimensions that are typically difficult to identify during site investigations. The simulated fault slip was then used to estimate the maximum seismic moment (M_0) based on the seismological theory proposed by Hanks and Kanamori (1979). Mortezaei and Vahedifard (2015) indicates that thinner reservoirs are associated with a higher probability of fault reactivation and tend to generate larger seismic events. Higher reservoir permeability can reduce the likelihood of fault reactivation, while higher reservoir porosity is associated with a longer rupture duration.

Rutqvist et al.(2007) employed a coupled model to evaluate the maximum injection pressure for CO_2 storage. The analysis was conducted using TOUGH-FLAC, a simulation tool developed by Rutqvist that integrates TOUGH2 for fluid flow analysis with FLAC3D for geomechanical analysis, enabling direct coupling of hydro-mechanical processes. The results demonstrated that simplified analytical solutions tend to underestimate or overestimate the maximum injection pressure (ranging from 20 MPa to 40 MPa) associated with fault slip induced by CO_2 injection, due to the inability of such solutions to incorporate critical geometric factors that influence the spatial distribution of fluid pressure and stress. In contrast, fully coupled numerical simulations provide a more accurate assessment of these variables, yielding a more reliable estimate of the maximum injection pressure, which was approximately 25 MPa in this study.

This study addresses these concerns by developing a multi-pronged technical framework to evaluate induced seismic risks at potential GCS sites. The Changhua Coastal Industrial Park in western Taiwan was selected as the pilot study area (Fig. 2), where detailed core samples and geological data are available. Although the project was canceled due to a combination of regulatory, technical, and public concerns, it still contributed valuable data. To assess whether CO_2 injection may compromise fault stability, a numerical model was used. The 3D Distinct Element Code (3DEC) enabled hydro-mechanical coupled simulations, following the recommendation of fully coupled numerical modeling by Rutqvist et al. (2007).

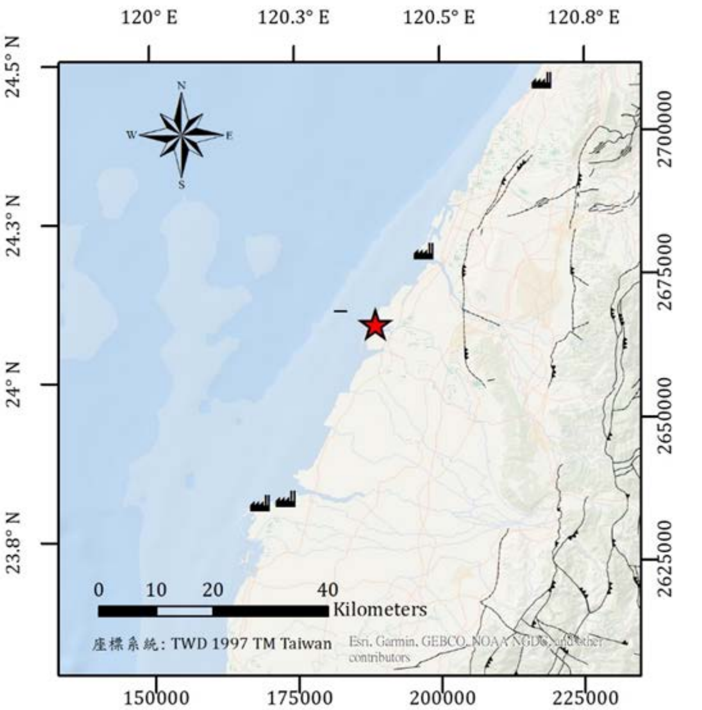

Fig. 2. The Changhua Coastal Industrial Park is shown in red star.

2. Methodology

To evaluate the potential for induced seismicity associated with CO_2 geological storage, a hydro-mechanical (HM) coupling model was developed using **3DEC version 7.0** (Itasca Consulting Group), which is particularly suited for modeling fractured rock masses through the Distinct Element Method (DEM). The target site, located in the Changhua Coastal Industrial Park, was represented using a stratified sedimentary model composed of alternating sandstone and shale layers, based on core and well-log data. This study conducted assessment of adjacent blind faults or fractures which may be reactivated under injection-induced stress perturbations.

According to the guidelines for the construction and application of the Engineering Geological Model (EGM) proposed by the International Association for Engineering Geology and the Environment (IAEG, 2022), two types of geological models were developed:

(1) Geological Model 1 (GM1): A simplified model assuming nearly horizontal stratigraphy with minimal dip, in which fault data are assumed (Fig. 3). A hypothetical fault (264 m x 264 m) 100 m is generated above injection point.

(2) Geological Model 2 (GM2): A refined model constructed based on geophysical data, incorporating curved stratigraphic surfaces and fault structures (Fig. 4). A normal fault (2 km x 2 km) based on reflect seismic profile is 5,700 m away from injection point.

The mesh was constructed using a nested tetrahedral grid, with higher resolution (100 m) near the injection point and coarser resolution (up to 1000 m) toward the model boundaries. A quarter-symmetry domain was adopted to reduce computational load. The CO_2 injection rate is set at 1 Mt/year, with an injection depth of 2,370 meters for both models.

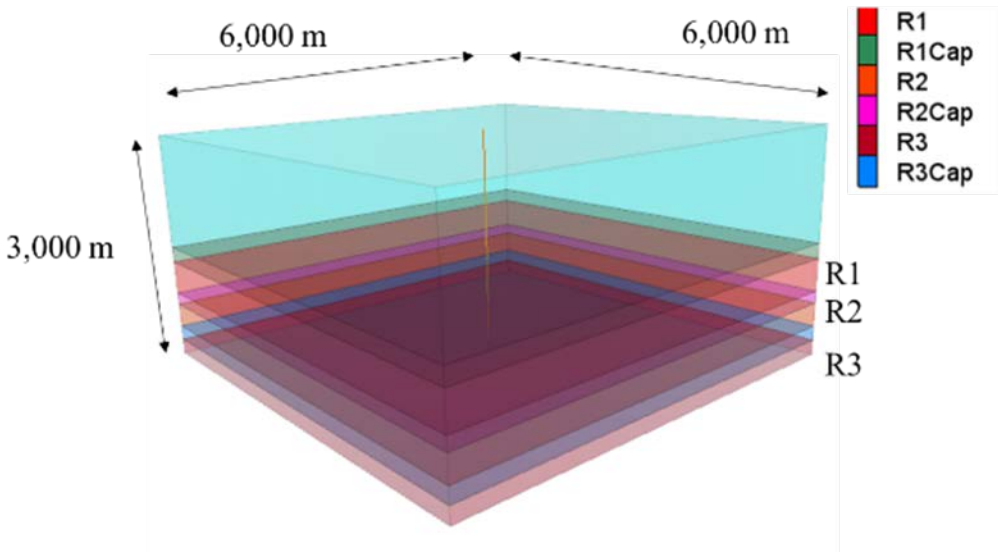

Fig. 3. Geological Model 1

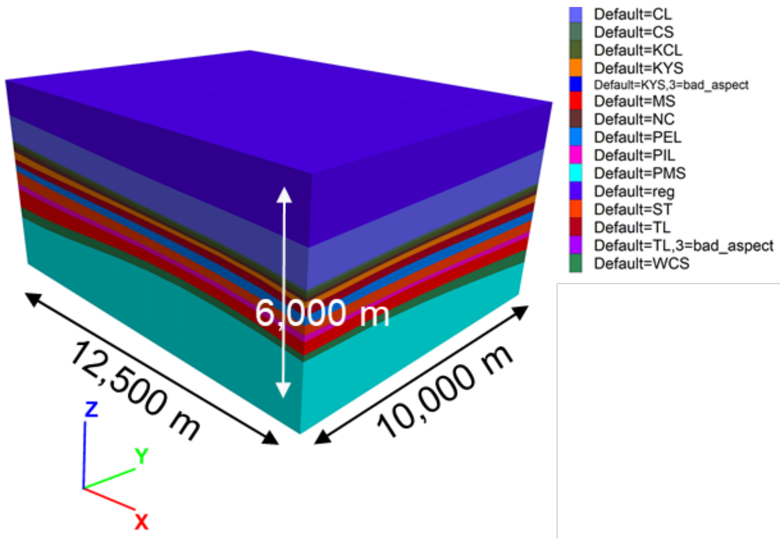

Fig. 4. Geological Model 2

3. Parameters

Based on the stratigraphic classification, the mechanical and hydraulic properties of the subsurface formations beneath the Changhua Coastal Industrial Park were defined as shown in Table 1 to Table 4. For faults near the injection site, the initial, minimum, and maximum aperture were all set to 1×10^{-4} m. Fluid flow simulations in 3DEC are limited to isotropic permeability, and anisotropic values cannot be directly input. Therefore, the geometric mean of the intrinsic permeability values was adopted for this study.

In addition, 3DEC uses the mobility coefficient, instead of intrinsic permeability for flow simulations. The required input parameter is converted using the following equation:

$$k_m = k/\mu \tag{1}$$

Where k is the intrinsic permeability and μ is the dynamic viscosity.

The density of the CO_2 fluid was set to 630 kg/m^3, and the dynamic viscosity was defined as 4.5×10^{-5} Pa·s.

According to SINOTECH (2014), the maximum principal stress is the vertical stress, indicating a normal faulting stress regime. Borehole breakout data derived from borehole wall resistivity imaging suggest that the minimum horizontal stress is oriented at 4.9°, while the maximum horizontal stress is oriented at 85.1°. The gradients of the maximum, intermediate, and minimum principal stresses are 22 MPa/km, 20 MPa/km, and 18 MPa/km, respectively.

The fault friction angle was set to 31°, and the fault cohesion was assumed to be 0 MPa for both mocel based on the study by Lin et al. (2017). The GM1 fault orientation was assumed to strike east–west and dip southward at 60°. The GM1 fault area was estimated using the empirical relationship proposed by Leonard (2014). To meet the seismic events to moment magnitude 3, the corresponding fault area is 0.07 km². Assuming a square-shaped fault, the resulting fault length and width are 264 meters. The GM2 fault is assumed to strike east–west, with a total length of 2 km and dipping northward. The dip angle is 35° in the upper section and 55° in the lower section, with a total fault area of approximately 4 km².

Table 1. Hydraulic Properties Input Parameters, GM1

Formation	Depth(m)	Porisity	Intrinsic permeability k_v (m^2)	Intrinsic permeability k_h (m^2)	Mobile coefficient k_m $(\frac{m^2 s}{Pa})$
Toukoshan Fm	0~1500	0.26	3.07e-14	9.21e-14	1.18E-09
R1Cap rock	1500~1700	0.26	3.07e-14	9.21e-14	1.18E-09
R1	1700~2135	0.26	3.07e-14	9.21e-14	1.18E-09
R2 Cap rock	2135~2295	0.23	3.33e-17	1.00e-16	1.28E-12
R2	2295~2608	0.24	Kueichulin Fm:7.31e-15 Kuanyinshan Fm:1.35e-14	Kueichulin Fm :2.91e-14 Kuanyinshan Fm:4.05e-14	4.10E-10
R3 Cap rock	2608~2800	0.2	上 4.66e-16 中 1.59e-14 下 8.9e-15	上 1.4e-15 中 4.77e-14 下 2.67e-14	1.56E-10

Table 2. Mechanical Properties Input Parameters, GM1

Formation	Depth(m)	Density	Bulk modulus (Pa)	Shear modulus (Pa)	Cohesion (Pa)	Friction angle	Tensile strength (Pa)
Toukoshan Fm	0~1500	2280	7.95E8	4.10E8	1.3E6	47	1.09E6
R1Cap rock	1500~1700	2270	1.25E9	4.49E8	1.00E6	43	4.93E5
R1	1700~2135	2270	1.25E9	4.49E8	1.00E6	43	4.93E5
R2 Cap rock	2135~2295	2320	1.29E9	7.35E8	2.08E6	45	1.26E6
R2	2295~2608	2245	1.00E9	4.00E8	2.00E6	44	5.30E5
R3 Cap rock	2608~2800	2425	2.36E9	1.84E9	2.82E6	44	1.16E6

Table 3. Hydraulic Properties Input Parameters, GM2

Formation	Depth(m)	Porisity	Intrinsic permeability k_v (m^2)	Intrinsic permeability k_h (m^2)	Mobile coefficient

					k_m $(\frac{m^2 s}{Pa})$
Toukoshan Fm	0	933.91	0.26	3.07e-14	9.21e-14
Cholan Fm	933.91	2597.24	0.26	3.07e-14	9.21e-14
Chinshui Sh	1727.62	2670.99	0.23	3.33e-17	1.00e-16
Kueichulin Fm	1770.35	2794.75	0.24	7.31e-15	2.91e-14
Nanchuang Fm	1899.71	2881.18	0.24	9.93E-15	3.43E-14
Kuanyinshan Ss	2089.62	3092.72	0.24	1.35e-14	4.05e-14
Talu Sh	2281.59	3404.09	0.2	top 4.66e-16 mid 1.59e-14 bottom 8.9e-15	top 1.4e-15 mid 4.77e-14 bottom 2.67e-14
Peiliao Fm	2462.35	3717.87	0.2	1.17e-15	3.51e-15
Shiti Fm	2651.92	4018.82	0.26	1.36728E-13	1.36728E-13
Piling Sh	2997.47	4243.14	0.25	2.14008E-14	2.14008E-14
Mushan Fm	3143.23	4925.06	0.25	2.14008E-14	2.14008E-14
Wuchishan Fm	3417.14	5490.53	0.25	2.14008E-14	2.14008E-14

Table 4. Mechanical Properties Input Parameters, GM2

Formation	Depth(m)	Density	Bulk modulus (Pa)	Shear modulus (Pa)	Cohesion (Pa)	Friction angle	Tensile strength (Pa)
Toukoshan Fm	2280	7.95E8	4.10E8	1.3E6	47	1.09E6	
Cholan Fm	2270	1.25E9	4.49E8	1.00E6	43	4.93E5	
Chinshui Sh	2320	1.29E9	7.35E8	2.08E6	45	1.26E6	
Kueichulin Fm	2245	1.00E9	4.00E8	2.00E6	44	5.30E5	
Nanchuang Fm	2245	1.00E9	4.00E8	2.00E6	44	5.30E5	
Kuanyinshan Ss	2245	1.00E9	4.00E8	2.00E6	44	5.30E5	
Talu Sh	2425	2.36E9	1.84E9	2.82E6	44	1.16E6	
Peiliao Fm	2427	3.20E9	2.26E9	5.90E6	48	2.25E6	
Shiti Fm	2427	3.20E9	2.26E9	5.90E6	48	2.25E6	
Piling Sh	2427	3.20E9	2.26E9	5.90E6	48	2.25E6	
Mushan Fm	2427	3.20E9	2.26E9	5.90E6	48	2.25E6	
Wuchishan Fm	2427	3.20E9	2.26E9	5.90E6	48	2.25E6	

4. Boundary condition

As the simulation process is divided into two stages, two sets of boundary conditions were applied. In the equilibrium stage, the lateral boundaries of the model had zero velocity in the x and y directions. The bottom boundary was defined as a roller boundary, while the ground surface was treated as a free boundary.In the injection stage, the ground surface remained a free boundary, while all other boundaries were set as viscous boundaries. Regarding fluid boundary conditions, all boundaries in 3DEC are impermeable by default. In this study, fixed groundwater pressure was applied to all boundaries except the ground surface.

5. Results

After five years of CO_2 injection, the east–west cross-sectional distribution of pressure buildup is shown in Fig. 5. The lateral extent of pressure increase (greater than 0.01 MPa) is primarily confined within 1.5 km in the east–west direction. The overlying R2 caprock exhibits good sealing capacity, resulting in pressure buildup occurring mainly below the R2 caprock in the vertical direction. The maximum pressure increase occurs at the injection point, reaching approximately 0.17 MPa.

Monitoring points were placed at the injection location, to record pressure evolution over time, as shown in Fig. 6. It is worth noting that although 3DEC does not support two-phase flow simulations and cannot capture the detailed migration of CO_2 plumes, the results of pressure magnitude and spatial extent of pressure changes are comparable to Mathias et al. (2009) approximate solutions.

The pressure buildup for GM1 and GM2 are 0.17 MPa and 0.18 MPa, respectively, showing no significant difference, as illustrated in Fig. 7. Notably, in the GM2, the influence of the dip angle of the Chinshui Shale caprock can be observed.

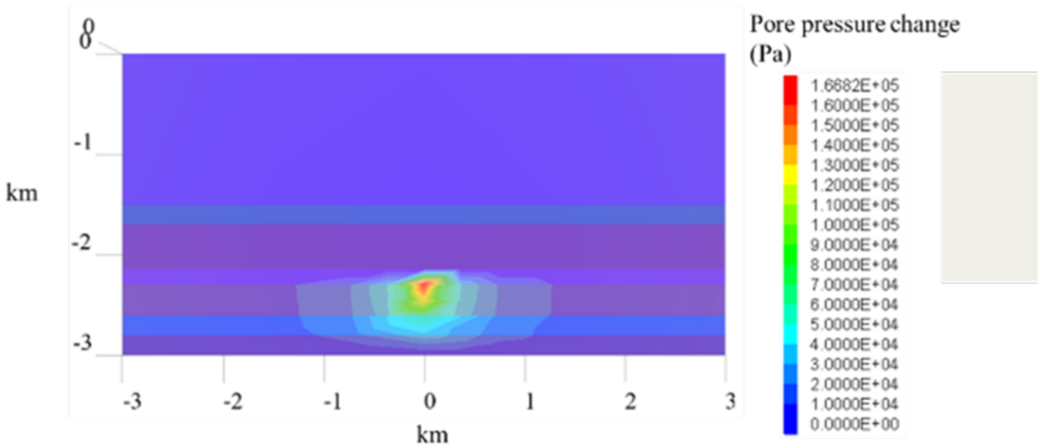

Fig. 5. Pressure buildup distribution after five tears of injection in GM1

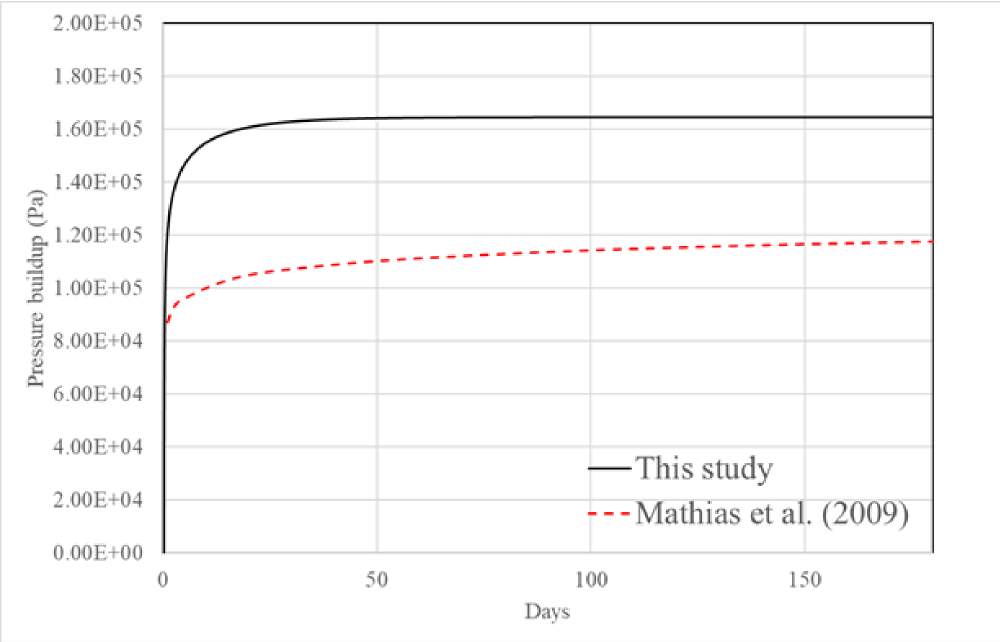

Fig. 6. Pressure buildup evolution over time.

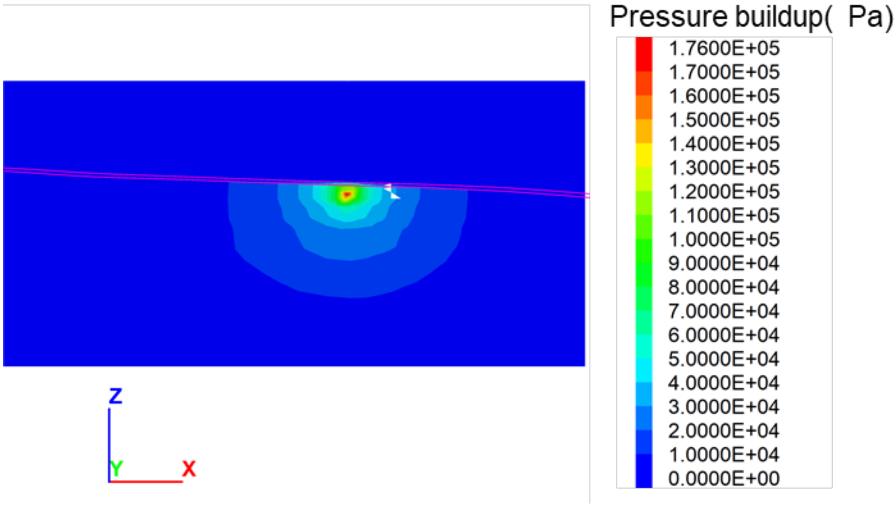

Fig. 7. Pressure buildup distribution after five tears of injection in GM2

GM1 assuming that a nearby blind fault is located within the R2 caprock above the injection point, at a distance of 100 meters (as shown in Fig. 8). It can be observed that the locations of maximum normal displacement and maximum shear displacement both occur at the lower-left corner of the fracture. This is because the lower-left corner is the closest point to the injection location. The temporal evolution of normal and shear displacements at this point is shown in Fig. 9. The maximum normal displacement is approximately 31 μm (indicating fracture opening), while the maximum shear displacement is approximately 6 μm.No shear or tensile failure was observed on the fracture plane; the relative displacements remained within the elastic deformation range.

The shear displacement along the fault plane for GM2 is shown in Fig. 10. The maximum shear displacement occurs near the center of the fracture. The magnitude of shear displacement is approximately 2.7 μm. No shear or tensile failure was observed on the fracture surface; the relative displacement shows a tendency toward reverse faulting but remains within the elastic deformation range.

Interestingly, despite the distances from the injection point to the fracture being 100 meters and 5,700 meters in the two models, respectively, the maximum shear displacements were of a similar magnitude. This discrepancy appears unreasonable and is presumed to result from numerical convergence errors or issues related to the mesh model, such as element size or connectivity.

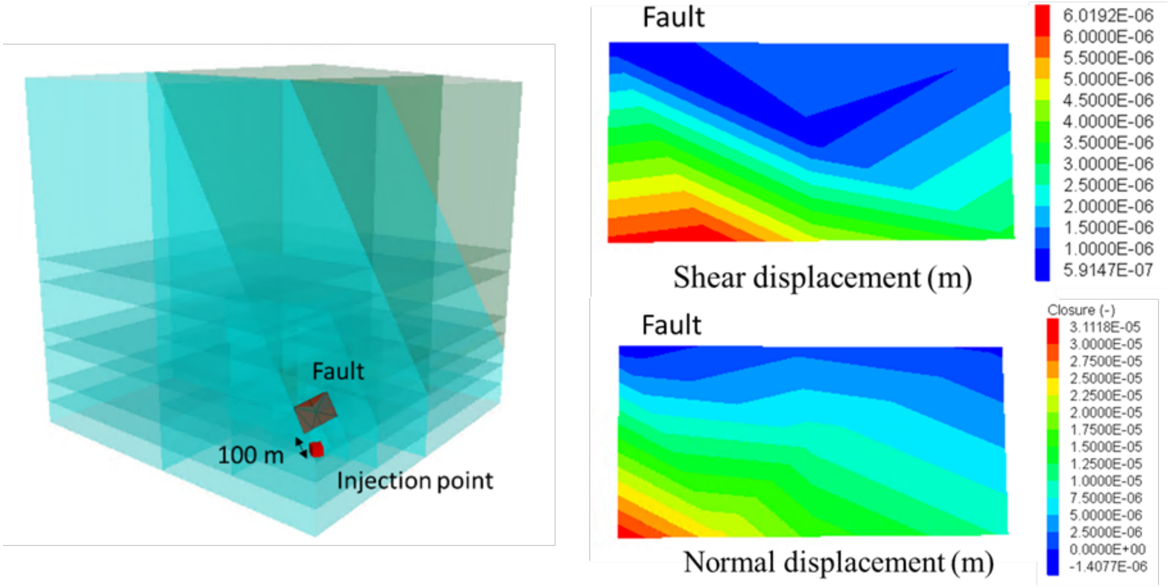

Fig. 8. Normal and shear displacement of fault in GM1

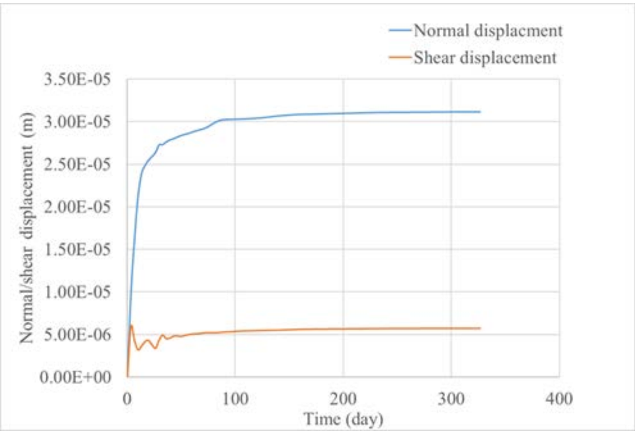

Fig. 9. Normal and Shear Displacement vs. Time on the Fracture Plane

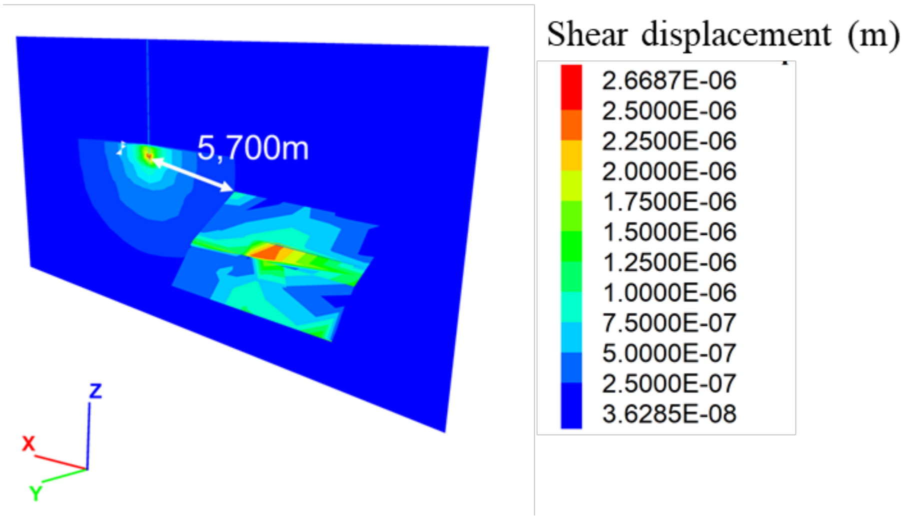

Fig. 10. Shear displacement of fault in GM2

To investigate the effects of two-phase flow during CO_2 injection into a saline aquifer, this study incorporated the Buckley–Leverett equation into the 3DEC model through the development of custom callback functions. These functions account for factors such as relative permeability, fluid viscosity, and the relationship between discharge and fluid saturation, while neglecting gravity and capillary forces.

The simulation result of injection point pressure is shown in Fig. 11. An overpressure is observed at the early stage of CO_2 injection, which is attributed to the very low relative permeability to CO_2. This phenomenon was also reported by Villarrrasa et al. (2016). In other words, pressure buildup under two-phase flow conditions is significantly higher than that observed in single-phase flow. Consequently, employing simplified single-phase flow models for CO_2 injection simulations may underestimate the actual pressure response and, in turn, the associated geomechanical risks.

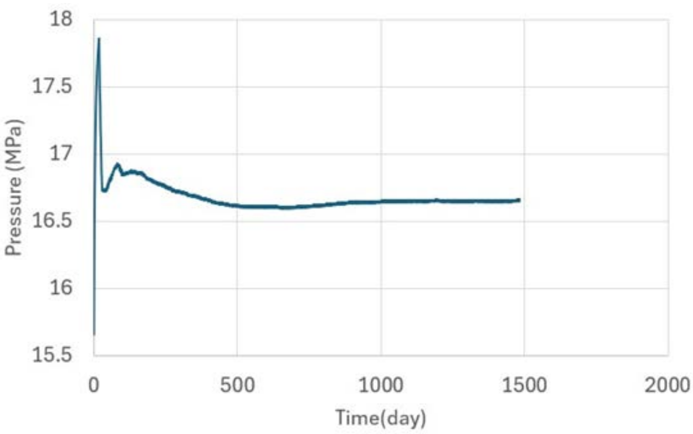

Fig. 11. Pressure evolution over time.

6. Conclusion and future work

Based on single-phase fluid flow simulations at an injection rate of 1 Mt/year, the adjacent faults (Model 1 and Model 2) at the Changhua Coastal Industrial Park CCS pilot site remain stable. However, a comparison with two-phase flow simulations using the Buckley–Leverett equation reveals that pressure buildup is significantly higher under two-phase conditions. An overpressure phenomenon is also observed during the early stages of CO_2 injection, primarily due to the low relative permeability to CO_2.

To improve the accuracy of geomechanical assessments, it is recommended to continue developing and integrating two-phase flow capabilities into 3DEC, including the effects of gravity and capillary forces, in order to better evaluate their influence on fault stability.

7. Acknowledgements

This research was supported by the National Science and Technology Council (NSTC), Executive Yuan, Taiwan, under the project "CO2 sequestration performance assessment of induced Seismicity" (Project No. NSTC 112-3111-Y-042A-001).

References

1. IEA (2017), Energy Technology Perspectives 2017, IEA, Paris https://www.iea.org/reports/energy-technology-perspectives-2017, License: CC BY 4.0.
2. Mortezaei, K., Vahedifard, F. (2015), Numerical Simulation of Induced Seismicity in Carbon Capture and Storage Projects, Geotech Geol Eng, 33:411–424, DOI 10.1007/s10706-015-9859-7.
3. Rutqvist, J. (2012), The Geomechanics of CO2 Storage in Deep Sedimentary Formations, Geotechnical and Geological Engineering, Vol. 30, pp. 525-551.
4. Hanks, T.C., Kanamori, H. (1979), A moment magnitude scale, Journal of Geophysical Research: Solid Earth, Vol. 84, pp.2348-2350.
5. Rutqvist, J., Birkholzer, J., Cappa F., Tsang, C-F. (2007), Estimating maximum sustainable injection pressure during geological sequestration of CO2 using coupled fluid flow and geomechanical fault-slip analysis, Energy Conversion and Management, Vol. 48, pp. 1798-1807.
6. IAEG (2022), Guidelines for the development and application of engineering geological models on projects, International Association for Engineering Geology and the Environment (IAEG), Commission 25 Publication No. 1, 129 pp.
7. SINOTECH (2014). Geological investigation and technology development for the pilot CO_2 geological storage site. Final report commissioned by Taiwan Power Company.
8. Lin, D.-S., Wang, C.-Y., Hsu, S.-K., Ni, C.-F., Jao, J.-C., Hsieh, P.-C., & Yang, K.-M. (2017). Investigation of potential CO_2 geological storage sites in onshore and offshore central Taiwan and planning for CCS development. Final report of a research project funded by the Ministry of Science and Technology, Taiwan.
9. Leonard, M. (2014), Self-Consistent Earthquake Fault-Scaling Relations: Update and Extension to Stable Continental Strike-Slip Faults, Bulletin of the Seismological Society of America, Vol. 104, No. 6, pp. 2953–2965, December 2014, doi: 10.1785/0120140087.

10. Mathias, S.A., Hardisty, P.E., Trudell, M.R., and Zimmerman, R.W. (2009) Approximate Solutions for Pressure Buildup duringCO2 Injection in Brine Aquifers, Transp Porous Med, 79, 265-284.
11. Villarrrasa, V., Carrera, J., & Olivella, S. (2016). Two-phase flow effects on the CO_2 injection pressure evolution and implications for the caprock geomechanical stability. E3S Web of Conferences, 9, 04007. https://doi.org/10.1051/e3sconf/20160904007.